Therapeutic Advances in Ophthalmology Review

Advances in multimodal imaging in ophthalmology

Ther Adv Ophthalmol
2021, Vol. 13: 1–22
DOI: 10.1177/25158414211002400

Morgan J. Ringel, Eric M. Tang and Yuankai K. Tao

***Abstract*:** Multimodality ophthalmic imaging systems aim to enhance the contrast, resolution, and functionality of existing technologies to improve disease diagnostics and therapeutic guidance. These systems include advanced acquisition and post-processing methods using optical coherence tomography (OCT), combined scanning laser ophthalmoscopy and OCT systems, adaptive optics, surgical guidance, and photoacoustic technologies. Here, we provide an overview of these ophthalmic imaging systems and their clinical and basic science applications.

Keywords: adaptive optics, multimodal, ophthalmic imaging, optical coherence tomography, scanning laser ophthalmoscopy

Received: 21 January 2021; revised manuscript accepted: 23 February 2021.

Correspondence to:
Yuankai K. Tao
Department of Biomedical Engineering, Vanderbilt University, Nashville, TN 37235, USA
yuankai.tao@vanderbilt.edu

Morgan J. Ringel
Eric M. Tang
Department of Biomedical Engineering, Vanderbilt University, Nashville, TN, USA

Introduction

Since the first demonstration of fundus photography, technological advancements have allowed for increasingly high-resolution and high-contrast imaging of the anterior and posterior eye. Development of scanning laser ophthalmoscopy (SLO) in 1980 allowed for en face retinal imaging with significantly reduced light exposure compared with conventional indirect ophthalmoscopy, with recent advancements focused on providing an ultra-wide field of view (FOV).[1–3] The introduction of optical coherence tomography (OCT) in 1991 enabled depth-resolved volumetric imaging, further facilitating ophthalmic disease diagnosis by providing access to subsurface features.[4] Adaptive optics (AO) was first introduced for fundoscopy in 1997 and has since been applied to both OCT and SLO to achieve cellular-resolution ophthalmic imaging by correcting aberrations of the eye.[5] Recent advances have focused on supplementing structural contrast with functional modalities, such as OCT-based quantification of the metabolic and biomechanical properties of ocular tissue and multimodality systems such as OCT-SLO, surgical microscope–integrated OCT, and multimodal photoacoustic microscopy (PAM). Here, we provide an overview of these ophthalmic imaging systems and their clinical and basic science applications (see Table 1).

OCT-derived contrast mechanisms

OCT is the clinical standard for diagnosing and monitoring ophthalmic diseases and enables subsurface visualization of tissue scattering. A combination of system modifications and post-processing algorithms can be applied to achieve a variety of complementary imaging modes that probe additional contrast mechanisms. Examples of these multimodal OCT techniques include optical coherence tomographic angiography (OCTA), polarization-sensitive OCT (PS-OCT), optical coherence elastography (OCE), phase-decorrelation OCT (PhD-OCT), photothermal OCT (PT-OCT), and pump-probe OCT (PP-OCT).

Optical coherence tomographic angiography

Changes to retinal vascular density and perfusion accompany many ophthalmic diseases, including glaucoma, age-related macular degeneration (AMD), and diabetic retinopathy (DR).[6] Fluorescein angiography (FA) and indocyanine green angiography (ICGA) have traditionally been used to detect vascular leakage, neovascularization, and occlusions.[7] However, these techniques require injection of exogenous contrast and lack depth selectivity for specific retinal layers.[8] Several different OCT acquisition and post-processing methods, collectively termed OCTA, have emerged as non-invasive alternatives for volumetric imaging of

Table 1. Summary of multimodal ophthalmic imaging technologies.

Technology	Application	*In vivo* ophthalmic human demonstration	Commercially available clinical system	Clinical or research focus
OCT angiography	Vascular imaging	Yes	Yes	Clinical
Polarization-sensitive OCT	Tissue depolarization and birefringence	Yes	No	Research
Optical coherence elastography Phase-decorrelation OCT	Tissue biomechanics	Yes	No	Research
Photothermal OCT Pump-probe OCT	Molecular contrast	No	No	Research
OCT + Scanning laser ophthalmoscopy	Motion-tracking	Yes	Yes	Clinical
Surgical visualization	Surgical imaging	Yes	Yes	Clinical
Photoacoustic imaging	Vascular imaging	No	No	Research

OCT, optical coherence tomography.

retinal vascular perfusion. Doppler OCT uses phase differences between repeated OCT acquisitions to estimate Doppler frequency shift and the relative velocity of flowing scatterers within perfused vessels.[9] However, phase-based angiography techniques are highly susceptible to bulk motion, which reduces sensitivity to blood flow. Power-Doppler methods, including optical micro-angiography (OMAG),[10,11] phase variance,[12] and Doppler variance angiography,[13] trade off flow velocity resolution for reduced sensitivity to bulk motion. These methods have demonstrated benefits for high resolution *in vivo* imaging of retinal and choroidal perfusion. Intensity-based angiography methods, such as split-spectrum amplitude-decorrelation angiography (SSADA)[14] and speckle decorrelation,[15] use intensity changes between repeated OCT cross sections as surrogate measures of blood flow and have been translated for clinical imaging of changes in optic disk perfusion in glaucoma and choroidal neovascularization in AMD patients.[16–19] Angiography methods that take advantage of both the amplitude and phase of the OCT signal further enhance robustness against phase instability and include complex differential variance (CDV)[20,21] and eigenvalue decomposition.[22] SSADA and OMAG have been integrated into commercially available systems (Optovue AngioVue and Zeiss AngioPlex, respectively), enabling high-quality clinical imaging and quantification of retinal perfusion.[23,24]

Handheld OCTA. Despite commercialization of OCTA, the majority of these systems require patients be imaged upright, thus precluding imaging in supine or bedridden patients. To address these limitations, several handheld OCT probes have been developed for point-of-care imaging,[25,26] including in pediatric patients.[27] Commercially available handheld OCT devices, such as the iVue (Optovue, Inc, Fremont, CA, USA) and Envisu C2300 (Leica Microsystems, GmbH, Wetzlar, DE), have relatively slow imaging speeds that limit sampling density and OCTA sensitivity. Research prototypes optimized for OCTA imaging[28–30] increase speeds by an order of magnitude compared with current-generation commercial systems by using 100–400 kHz swept sources. Clinical imaging of retinopathy of prematurity (ROP) patients using these systems has provided *in vivo* images of the foveal avascular zone and retinal capillary complex in neonates (Figure 1(a)–(d)).[31,32]

Visible-light OCTA. Ophthalmic OCT has conventionally been performed using near-infrared wavelengths because of the availability of light sources and benefits in reduced scattering and increased penetration depths. Commercial availability of broadband supercontinuum light sources has enabled OCT imaging at visible wavelengths, which provides access to more endogenous and exogenous molecular contrast mechanisms.[33–38] When combined with OCTA

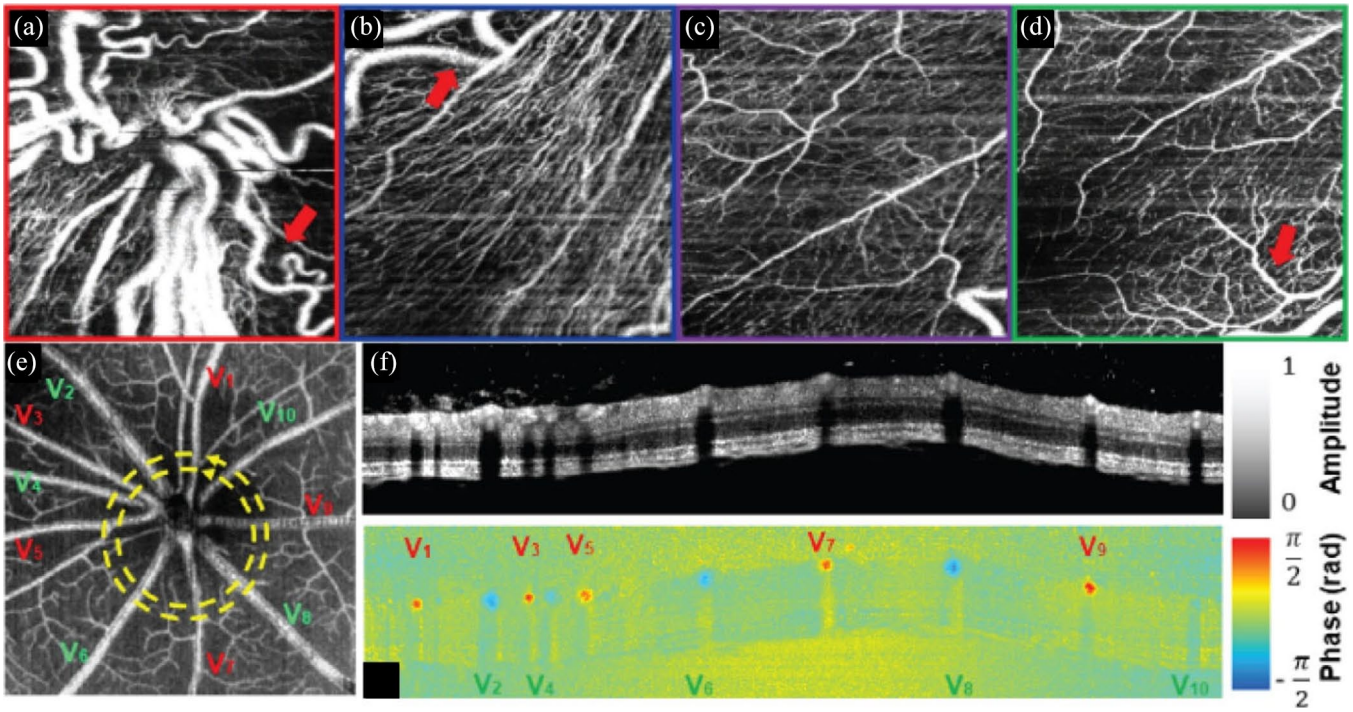

Figure 1. (a)–(d) Handheld OCTA of ROP at the (a) optic nerve head, (b) peripapillary region, (c) perifoveal region, and (d) margin of the fovea. Visible-light OCT in a rodent model showing (e) OCTA projection with delineation of arteries (red) and veins (green), and circumpapillary (f) retinal structure and (g) Doppler blood flow cross section.
Source: Reprinted with permission from Viehland and colleagues[31] and Pi and colleagues.[43]
OCT, optical coherence tomography; OCTA, optical coherence tomographic angiography; ROP, retinopathy of prematurity.

maps of retinal vascular perfusion, visible-light OCT can provide complementary contrast for quantifying blood oxygenation as a surrogate for quantifying metabolic changes associated with DR and AMD (Figure 1(e)–(g)).[36,38–45] *In vivo* visible-light OCT retinal imaging has been demonstrated, and development of robust clinical systems is ongoing.[36,46–48]

Clinical utility and challenges. Ongoing clinical OCTA research focuses on imaging in AMD, DR, and diabetic macular edema (DME) and vascular response to therapy or surgery.[49–52] Wide-field OCTA systems have also been developed and are capable of imaging a 100° FOV, which benefits imaging of the peripheral retina.[53,54] Despite significant advantages over FA and ICGA, the clinical utility of OCTA is limited by several key factors. Engineering advancements in OCTA algorithms require physician education for proper interpretation of angiograms.[55] OCTA algorithms also require repeated imaging and dense sampling over small FOVs, making them susceptible to bulk motion during long acquisitions. Handheld OCTA imaging is further complicated by combined patient and photographer motion, both of which degrade vascular contrast and resolution, distort anatomic features, and preclude robust quantitative measurements.[31,56] Additional image artifacts, such as shadowing from large retinal vessels, axially smeared vessel cross sections as a result of scattering, and out-of-focus OCTA projections, can significantly impact vessel segmentation algorithms and quantitative analysis of retinal vascularity.[57–60] Motion-compensation methods, such as novel scanning or eye-tracking technologies, are actively being studied to overcome these limitations.[61–64] Furthermore, vessel enhancement techniques, such as the complex continuous wavelet transform and multiple en face registration and averaging, can be applied to improve the accuracy of vessel segmentation.[65–68] Despite these methods, various commercial systems employ different post-processing and segmentation algorithms, making interpretation by clinicians challenging.[7] While visible-light OCT provides complementary endogenous functional contrast, clinical translation of the technology is challenging because visible wavelengths are distracting and make fixation extremely difficult.[48] In

addition, visible-light OCT images routinely require dense averaging to overcome low image quality that results from higher laser noise and significantly lower maximum permission exposure compared with near-infrared sources.[69]

Polarization-sensitive OCT

PS-OCT measures changes in polarization states between incident and back-reflected light, which can provide additional tissue-specific contrast.[70] The amplitude and relative phase delay between orthogonal polarization states can be used to compute parameters such as tissue birefringence and degree of polarization uniformity.[71–77] These methods enable quantitative *in vivo* imaging of changes in tissue properties resulting from disease progression and treatment.[78,79]

Anterior segment. PS-OCT is particularly well suited for corneal imaging because the collagen stroma exhibits strong birefringence.[80] Previous works have shown that corneal birefringence is related to fibril orientation in the lamellae, and quantitative metrics, such as phase retardation and slow axis orientation, have been used to distinguish healthy from diseased corneas.[81,82] Keratoconus, which is characterized by thinning and distortion of the central cornea, exhibits increases in phase retardation near the rim of corneal thinning and changes in slow axis orientation resulting from rearrangement of stromal collagen.[83] PS-OCT can also enhance visualization of the trabecular meshwork, ciliary body, and iris, which can be used to study the progression of diseases such as glaucoma.[84–86] Excess buildup of aqueous humor because of glaucoma can require surgical intervention, commonly trabeculectomy, which allows for aqueous flow into the subconjunctival space. Post-operative PS-OCT has characterized intra-bleb fibrosis and associated complications to benefit clinical management after trabeculectomy.[87,88] Improvements in OCT speed and resolution have benefited PS-OCT by enabling quantitative measurement of corneal layer thicknesses and enhanced visualization of Bowman's membrane and the sub-basal nerve plexus.[89–92]

Posterior segment. PS-OCT in the posterior segment has traditionally measured retinal nerve fiber layer (RNFL) birefringence and thickness.[81,93–95] Similar to the cornea, bundles of parallel cylindrical axons in the RNFL exhibit high birefringence, and decreases in RNFL birefringence can potentially be used as a surrogate measure for ganglion cell and axonal atrophy in glaucoma.[96] Similar changes in phase retardation and birefringence resulting from RNFL thinning have been observed in diabetic eyes (Figure 2).[97,98] PS-OCT characterization of the macula has shown that the retinal pigment epithelium (RPE) is highly depolarizing, scrambling the polarization of backscattered light from the RPE and choroid.[99,100] Studies have quantified the degree of polarization uniformity (DOPU) from PS-OCT images and used it to aid RPE segmentation and thickness mapping, which can benefit quantitative monitoring of drusen and geographic atrophy in AMD.[71,101–105] PS-OCT has also been used to detect and segment subretinal fibrosis, which is common in neovascular AMD and difficult to differentiate from other hyperreflective tissues.[106,107]

Clinical utility and challenges. The majority of PS-OCT research has focused on quantifying changes in tissue properties resulting from ophthalmic diseases. Polarization-sensitive OCTA has also been demonstrated for ophthalmic imaging using Jones matrix-based CDV.[21] The use of polarization-based angiography has advantages over conventional OCTA by improving vessel contrast and increasing image signal; four OCTA images (two incident and two detected polarization states) can be generated and averaged for increased SNR.[108] Despite the utility of PS-OCT in differentiating birefringent and depolarizing tissues in the eye, there are no commercially available PS-OCT systems routinely used in clinical ophthalmology. Challenges in clinical translation include increased cost and system complexity over conventional OCT systems. Many PS-OCT systems use free-space optics, which are sensitive to misalignment,[109] whereas fiber-based PS-OCT systems are more robust but are limited by birefringence and polarization mode dispersion of fiber-optic components.[110] One limitation of using depolarization maps for RPE segmentation is distinguishing it from the choroidal stroma. However, by combining PS-OCT with OCTA, the vessel-rich choroidal stroma can be separated from the vessel-free RPE and can be used to evaluate damage in the RPE layer due to serous RPE detachments.[111,112]

OCT elastography

OCE uses OCT imaging to detect micron-scale displacements caused by an external mechanical stimulus to extract biomechanical properties of tissue.[113,114] PhD-OCT is an alternate method for measuring tissue biomechanics that uses the

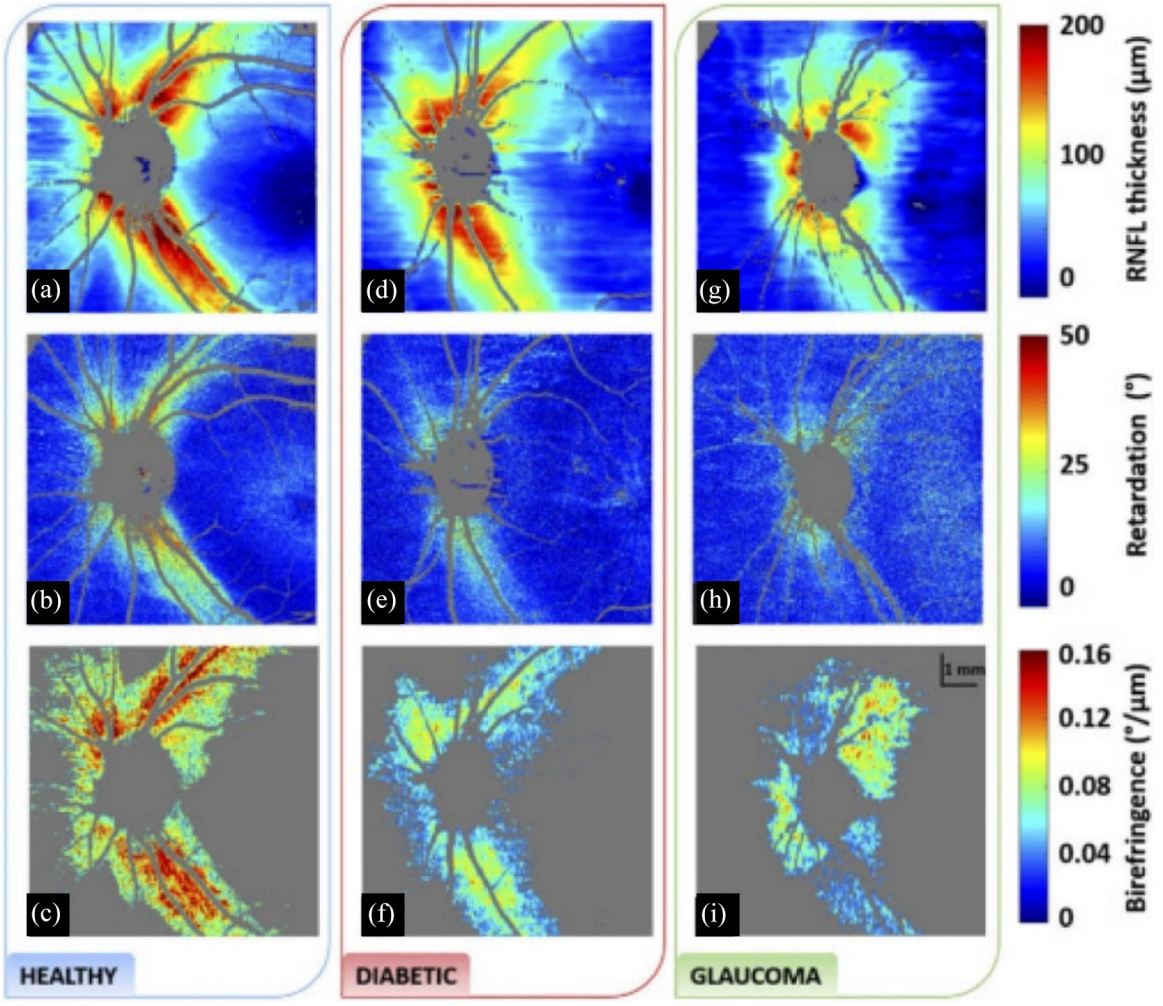

Figure 2. Comparison of (a), (d), (g) RNFL thickness, (b), (e), (h) phase retardation, and (c), (f), (i) birefringence between healthy, diabetic, and glaucoma subjects. Reduced retardance is seen in both diabetic and glaucoma subjects compared with healthy subjects. In addition, there is significantly reduced birefringence in diabetic patients.
Source: Reprinted with permission from Desissaire and colleagues.[98]
RNFL, retinal nerve fiber layer.

decorrelation of scattered light from Brownian motion as a surrogate measure of tissue viscosity.[115–117] Initial OCE demonstrations used OCT speckle tracking of axial displacements from a static loading force to quantify tissue strain and derived Young's modulus from the linear stress–strain relationship.[118,119] OCE can also be used to measure Young's and shear moduli by combining dynamic loading forces, such as steady-state harmonic loading and transient excitation sources, with advanced wave propagation models.[120] These dynamic OCE methods have been used to non-invasively measure biomechanical properties of the human cornea *in vivo*, showing the potential for clinical translation and utility.[121]

Cornea. Corneal elasticity can be a useful direct measure for diagnosing keratoconus and corneal ectasia and monitoring corneal collagen cross-linking (CXL) treatment.[122–125] The corneal elastic modulus changes with increased intraocular pressure (IOP) and can be used as an indirect measure for diagnosing glaucoma.[126] OCE has shown increased corneal stiffness in *in vivo* rabbit eyes after CXL treatments with an air puff as the external mechanical stimulus (Figure 3(a) and (b)).[127–129] OCE studies using air-coupled ultrasound excitation, which is non-contact and more applicable for clinical translation, have successfully shown quantitative 4-dimensional (4D) visualization of corneal stiffness.[130–133] More

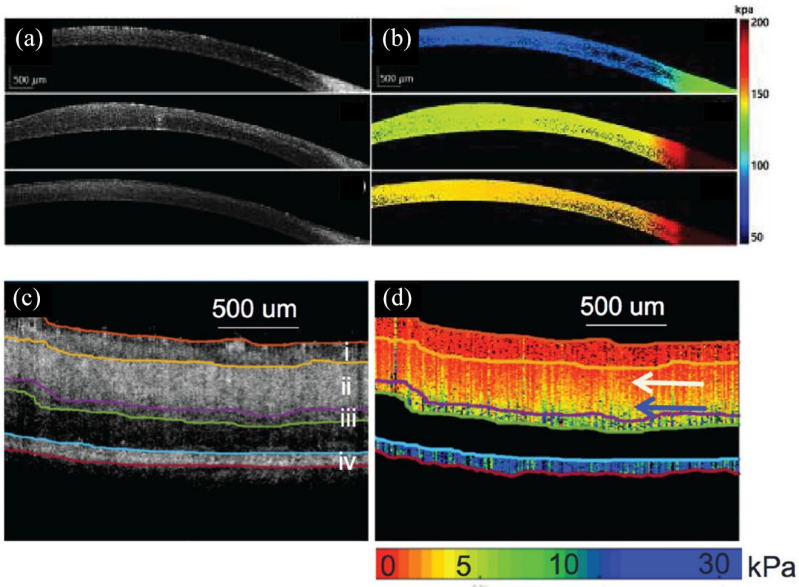

Figure 3. OCE imaging of the (a), (b), cornea and (c), (d) retina. (a) Structural OCT and (b) OCE elastogram cross sections of *in vivo* rabbit cornea pre-, post-, and 1 week after CXL treatment (top to bottom, respectively). (c) Structural OCT and (d) OCE elastogram cross sections of *ex vivo* porcine retina showing differences in retinal layer stiffness.
Source. Reprinted with permission from Zhou and colleagues[127] and Qu and colleagues.[142]
CXL, corneal collagen crosslinking; OCE, optical coherence elastography; OCT, optical coherence tomography.

recent OCE demonstrations have used acoustic radiation force (ARF) loading with an ultrasound transducer, which has a faster response time as compared with air puff loading.[134] Additional OCE stimuli include passive mechanical perturbations caused by the heartbeat[135] or using a pulsed laser to induce mechanical waves,[136] but these methods have yet to be demonstrated *in vivo*. PhD-OCT has successfully identified changes in corneal biomechanics after CXL *in vivo* without the need for external stimuli.[117]

Lens. OCE can offer a quantitative, non-invasive method for early detection and monitoring of changes in lens biomechanics associated with cataracts and aging.[137] ARF-OCE has shown higher Young's modulus in cataract lenses compared with healthy lenses in *ex vivo* rabbit eyes and significant increases in lens stiffness with aging *in vivo*.[138] OCE imaging has also been combined with Brillouin microscopy, which measures material stiffness using differences in Brillouin light scattering, to show a correlation between Young's and Brillouin moduli and provide a more complete mapping of lens stiffness in *ex vivo* porcine eyes.[139] Finally, OCE has also been used to investigate changes in lens elasticity as a function of IOP.[140]

Retina. Cellular changes in AMD can alter the elasticity of retinal tissue, making OCE a potential technology for early disease diagnosis.[141] ARF-OCE studies have shown distinct elasticity differences in retinal layers in *in vivo* rabbit and *ex vivo* porcine models (Figure 3(c) and (d)).[142,143] Decreased retinal stiffness observed in *in vivo* rabbit AMD eyes was hypothesized to result from lymphocyte infiltration, but initial results did not show statistical significance.[143] OCE studies have also shown that increased optic nerve head Young's modulus and posterior scleral stiffness are correlated with increasing IOP, which suggests that OCE can also be used to monitor progression of glaucoma.[144,145]

Clinical utility and challenges. Both OCE and PhD-OCT technologies are in the early stages of clinical translation, and current research is focused on improving imaging speed and phase stability.[146] Repeated images are used to compute differential phase in OCE, but this increases total imaging time and is susceptible to motion artifacts. Recent advances in swept-source OCT technology may overcome these limitations by enabling OCE imaging at megahertz rates.[147] Currently, there are no commercial OCE systems available for clinical use. The broad clinical adoption of OCT in ophthalmology may benefit clinical translation of multimodal OCE technologies pending successful identification of optimal mechanical stimulus mechanisms and clinical applications.

Molecular contrast methods

OCT sensitivity to changes in optical pathlength can be increased by leveraging phase information and used to probe additional mechanisms of contrast. As an example, light absorption by endogenous or exogenous contrast agents induces local temperature gradients and index of refraction changes. PT-OCT uses these index changes as a complementary contrast mechanism for detecting functional cellular and subcellular changes that could enable earlier disease detection.[148] PT-OCT has been demonstrated using exogenous gold nanoparticles and endogenous melanin in the RPE and choroid (Figure 4(a) and (b)) in *in vivo* and *ex vivo* animal models.[148–151] Most recently, PT-OCT using indocyanine green (ICG) was demonstrated as a method for

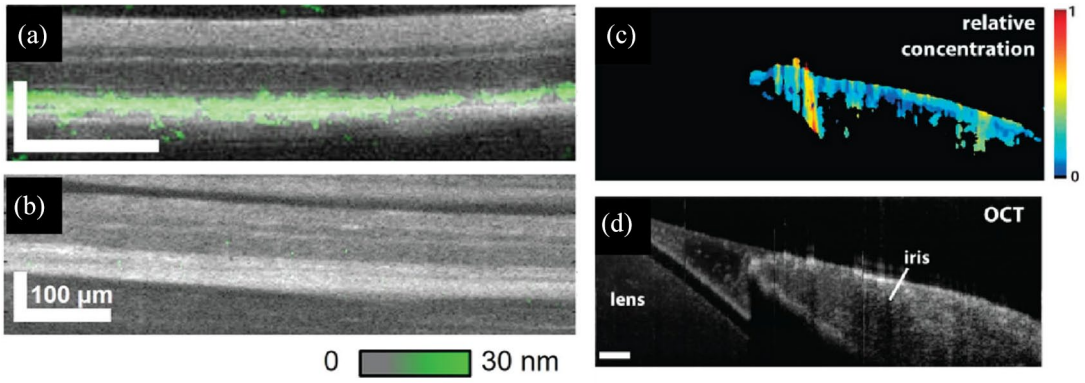

Figure 4. Molecular contrast imaging. *In vivo* PT-OCT comparing (a) pigmented to (b) albino mouse retina with computed melanin concentration (green) overlaid on OCT cross sections. PP-OCT image of *ex vivo* porcine iris showing the (c) relative concentration of melanin and (d) corresponding OCT cross section.
Source: Reprinted with permission from Lapierre-Landry and colleagues[150] and Jacob and colleagues.[155]
OCT, optical coherence tomography; PP-OCT, pump-probe OCT; PT-OCT, photothermal OCT.

distinguishing the inner limiting membrane, which is of interest for macular surgery applications.[152] PP-OCT is another technique for adding molecular contrast to OCT imaging. PP-OCT excites ground-state electrons using a modulated excitation (pump) and detects the transient absorption at a lower energy wavelength (probe) to identify specific molecular compounds such as methylene blue, hemoglobin, or melanin.[153,154] PP-OCT imaging in *ex vivo* porcine iris has demonstrated sensitivity to melanin, which may be a useful diagnostic tool for ocular melanoma (Figure 4(c) and (d)).[155]

Clinical utility and challenges. PT-OCT and PP-OCT are promising multimodal techniques that supplement OCT contrast, but neither have been demonstrated in *in vivo* human applications nor have commercialized clinical systems. Tissue heating and high excitation power levels are two safety concerns that need to be addressed. Acquisition speed is an additional limiting factor because of the need to critically sample the modulation frequency of the pulsed light source and slow heating response of absorbers.[152]

OCT-SLO

The inherent orthogonal priority acquisition orientations between OCT and SLO provide complementary depth-resolved and en face information that makes combined OCT-SLO an ideal multimodality technology. These systems can leverage fundus features for motion-tracking and volumetric imaging of anatomic structures and pathologies.

Tracking SLO

SLO has been used extensively for aiming and motion compensation of ophthalmic OCT.[156–159] Tracking SLO has been particularly critical for OCTA, which requires dense sampling over small FOVs and is, therefore, difficult to target ROIs and highly susceptible to saccadic and bulk motion artifacts.[62] Many current generation combined OCT-SLO systems use shared optics and scanners to relay light into the eye to reduce overall system complexity and provide pixel-level co-registration between corresponding OCT and SLO images.[160–163] SLO motion-tracking precision is related to both spatial and temporal resolution, and development of line-scanning SLO (LSLO) has overcome frame-rate limitations of conventional point-scanning SLO systems at the expense of full confocality, allowing imaging of fast dynamics up to several hundred frames per second.[163–166]

Handheld OCT-SLO

Multimodal OCT-SLO systems have traditionally been integrated with slit lamps that required patients to sit upright during imaging. The development of compact OCT-SLO handheld probes has benefited ophthalmic disease diagnostics in pediatric and bedridden patients.[27,167] When combined with a white-light supercontinuum light source, additional spectroscopic information can be extracted, including color SLO images that can be used to detect early signs of fundus discoloration in AMD.[168] Novel extended source LSLO illumination and detection schemes, such as those using spectral encoding, have replaced

complex free-space relays from source to detector with fiber optics, and handheld prototypes using these technologies have recently been used for motion-corrected *in vivo* ophthalmic OCT and OCTA.[30,169,170]

Adaptive optics

Lateral resolution in ophthalmic imaging is fundamentally limited by wavefront aberrations of the eye. AO overcomes this limitation by actively compensating for these aberrations using a deformable mirror, enabling cellular-resolution *in vivo* imaging.[5,171] Combined AO-SLO and AO-OCT systems are capable of imaging individual photoreceptors with up to two to three times higher transverse resolution than conventional SLO and OCT.[172–175] When combined with hardware- and software-based retinal-tracking technologies,[176] AO systems can be used to quantify retinal photoreceptor distributions across large FOVs and study cellular changes associated with retinal disease progression (Figure 5(a)–(f)).[103,177–207] In addition to structural imaging, AO systems have also demonstrated benefits for functional imaging, including visualizing perfusion in the retinal microvasculature and phase dynamics from photoreceptor photostimulation.[208–210]

Fluorescence SLO

The combination of SLO and fluorescence contrast is uniquely suited for high-specificity functional imaging in clinical ophthalmology and basic science. Traditional clinical applications have included fundus autofluorescence to detect endogenous fluorophores and exogenous fluorescein or ICG to visualize retinal vascular perfusion and leakage.[211] In animal models, combined OCT and fluorescence SLO systems enabled longitudinal imaging of retinal structure and characterization of function and cell populations in transgenic models expressing fluorescent proteins in serum albumin, microglia, and photoreceptors.[212,213] Animal models also provide an opportunity to study the effects of retinal injury, including laser-induced choroidal neovascularization, retinal vascular occlusion, laser lesioning, and image-guided intraocular drug-delivery.[214–217] One major limitation of fluorescence SLO is its limited depth-sectioning and volumetric imaging capability. Oblique SLO (oSLO) addresses this limitation by using obliquely oriented excitation and detection paths to acquire fluorescence cross sections and volumes (Figure 5(g)–(l)).[218] Fluorescence SLO can also be combined with AO to improve depth-sectioning and lateral resolution to enhance visualization of individual photoreceptors, ganglion cells, and RPE cells in animal models.[219–224]

Clinical utility and challenges

Combined OCT-SLO technology has been integrated into commercial systems, including the Heidelberg Spectralis, Optos Silverstone, and Zeiss PLEX Elite, for active motion-tracking and high-resolution en face and cross-sectional imaging of the fundus. While several AO systems, such as the Imagine Eyes rtx1 and Physical Sciences compact AO retinal imager (CAORI), are commercially available, broad adoption of the technology is limited because of system complexity, the need for long imaging and post-processing times, and lack of standardized processing and analysis algorithms.[225] Sensorless AO systems have been demonstrated in research prototypes and eliminate the need for physical wavefront sensors, which significantly reduces system complexity.[226–230] These technologies have been recently integrated into handheld probes for AO imaging in supine and pediatric patients, which may further motivate broad clinical adoption.[231,232] Fluorescence angiography and fundus autofluorescence are well established in clinical ophthalmology. More recently, autofluorescence lifetimes have been used as a surrogate for retinal metabolism that provides additional contrast for identifying ophthalmic and systemic diseases.[233–235]

Multimodal surgical visualization

Integration of OCT with ophthalmic surgical microscopy can provide additional high-resolution depth-resolved volumetric visualization of tissue microstructures that benefits surgical decision-making.[236] Initial demonstrations of intraoperative OCT (iOCT) were performed with handheld probes during surgery,[237–239] and the technology has since advanced to microscope-integrated systems that allow for OCT imaging concurrent with ophthalmic surgery.[240,241] Recent iOCT research has focused on improving speed and ergonomics, such as automated instrument-tracking and enhanced visualization. The combination of high-speed swept-source OCT systems with real-time volumetric rendering methods has allowed for 4D visualization of surgical dynamics

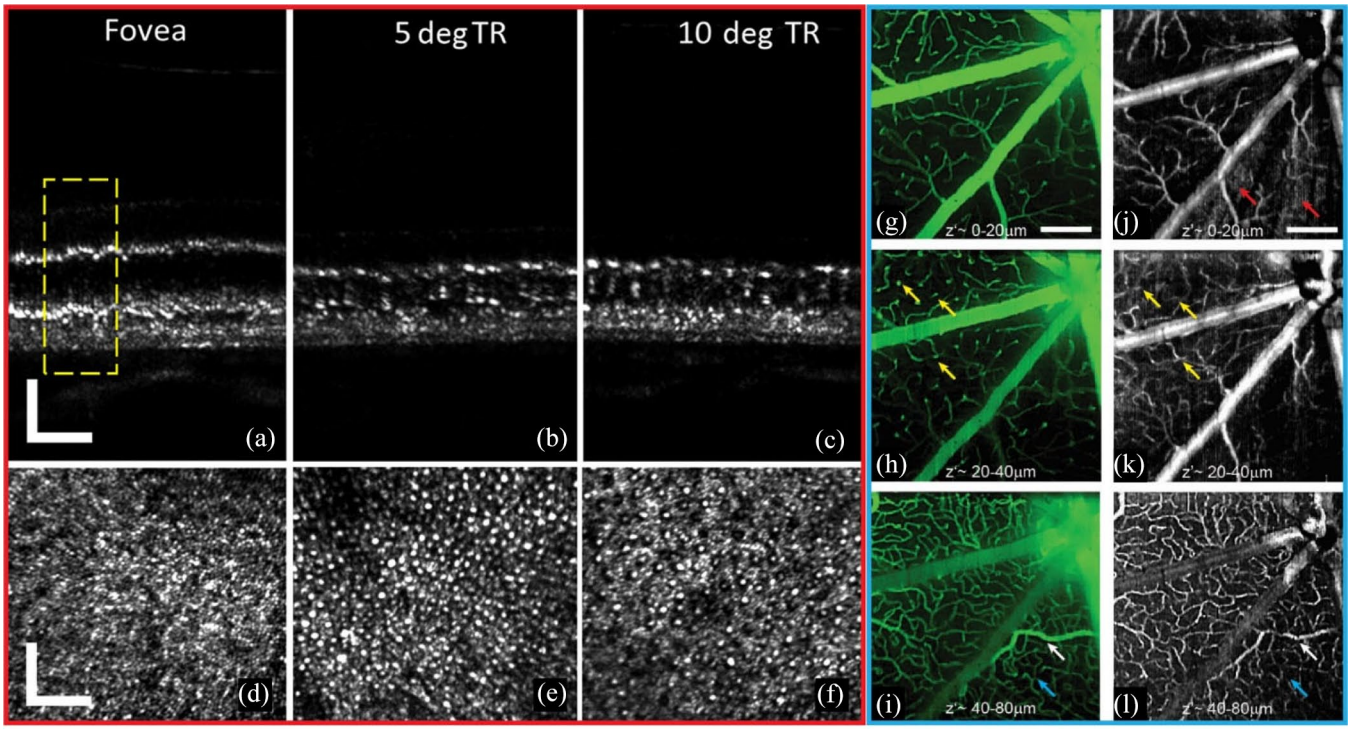

Figure 5. *In vivo* human (a)–(c) AO-OCT and (d)–(f) AO-SLO showing photoreceptors at (a), (d) the fovea, (b), (e) 5° TR, and (c), (f) 10° TR. Scale bar = 50 µm. (g)–(i) oSLO fluorescence projections and (j)–(l) corresponding OCTA projections showing murine retinal perfusion. Scale bar = 200 µm.
Source: Reprinted with permission from Wells-Gray and colleagues[201] and Zhang and colleagues.[218]
AO-OCT, adaptive optics OCT; AO-SLO, adaptive optics SLO; OCTA, optical coherence tomographic angiography; oSLO, oblique scanning laser ophthalmoscopy; TR, temporal retina.

(Figure 6(b)).[242–244] OCTA imaging has also been explored as a method for integrating vascular contrast to further enhance intraoperative visualization.[245,246]

Clinical utility and challenges

Multiple iOCT systems are commercially available, including the Haag-Streit Surgical iOCT, Zeiss RESCAN 700, and Leica EnFocus.[247] Clinical studies have shown that iOCT can benefit surgical decision-making for donor graft positioning during corneal transplant (Figure 6(a)) and during membrane peeling and retinal detachment repair procedures.[248,249] One major challenge in iOCT imaging has been shadowing from optically opaque surgical instruments. However, semi-transparent, OCT-compatible surgical instruments have been explored to overcome these limitations.[250] While preliminary studies have shown the benefits of iOCT for providing real-time surgical feedback, additional improvements in the technology are being developed, and studies demonstrating clinical utility are ongoing.

Photoacoustic imaging

Photoacoustic imaging detects acoustic waves generated by thermoelastic expansion from the absorption of pulsed laser illumination and reconstructs a volume of absorbers.[251,252] In ophthalmology, PAM primarily visualizes blood absorption and has advantages over FA and ICGA by not requiring exogenous contrast and OCTA by being sensitive to vascular leakage. PAM also has higher depth penetration compared with OCT and can achieve imaging depths exceeding 10 mm.[253] PAM demonstrations in animal models include visualization of deep retinal and choroidal vasculature, subretinal injections, and neovascularization.[254] Multimodal PAM and OCT imaging provides complementary structural and vascular contrast and has been used to visualize neovascularization in animal models of DR and wet-AMD.[255–259] Combined PAM and OCT has also shown advantages for visualizing vascular and structural changes associated with retinal vein occlusion (Figure 7) and choroidal vascular occlusion over FA.[260,261] Finally, PAM and OCT can be used to quantify

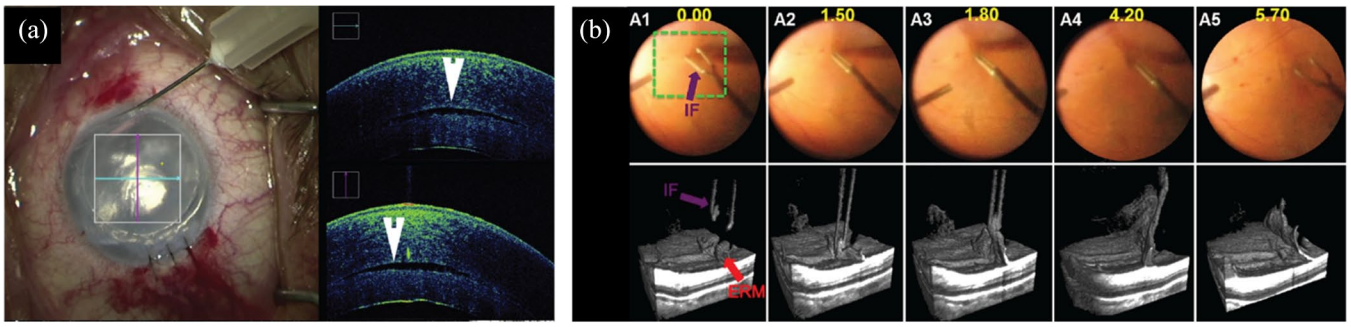

Figure 6. iOCT visualization during (a) anterior and (b) posterior segment surgery. (a) iOCT showing graft placement during corneal transplant showing a persistent fluid interface (arrowhead). (b) 4D iOCT imaging of forces peeling epiretinal membrane.
Source: Reprinted with permission from Carrasco-Zevallos and colleagues[243] and Ehlers and colleagues.[249]
4D, 4-dimensional; iOCT, intraoperative optical coherence tomography.

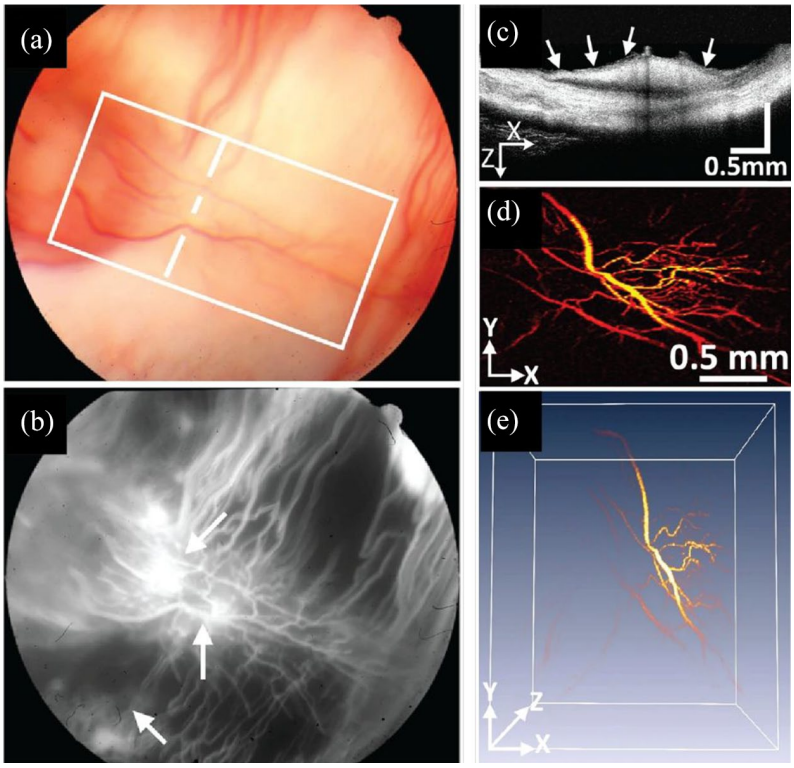

Figure 7. *In vivo* PAM showing neovascularization in rabbit retina. (a) Color fundus, (b) FA, (c) cross-sectional OCT, (d) PAM maximum amplitude projection, and (e) PAM 3D reconstruction of neovascularization (arrows).
Source: Reprinted with permission from Nguyen and colleagues.[260]
FA, fluorescein angiography; OCT, optical coherence tomography; PAM, photoacoustic microscopy; 3D, 3-dimensional.

retinal oxygen metabolism rates by combining blood flow measurements from Doppler OCT with hemoglobin oxygen saturation measured using multiwavelength PAM that may benefit early diagnosis of glaucoma, DR, and AMD.[39,262]

Clinical utility and challenges

Although there are commercial PAM systems such as the Vevo LAZR-X for cardiac and neuroimaging, PAM imaging systems for ophthalmic applications are not currently available.[263] Barriers to clinical translation of PAM include system complexity, slow imaging speeds, and the need for a contact-PAM transducer. Multimodal PAM and OCT requires dedicated laser sources for PAM excitation and OCT imaging, a transducer for PAM detection, and an OCT engine. Methods to share a laser source between PAM and OCT to reduce system complexity have been proposed. However, hemoglobin absorption is low in the near-infrared, which limits PAM sensitivity at OCT wavelengths.[264]

Conclusion

Multimodal ophthalmic imaging spans multiple optical and acoustic technologies. Many of these methods, such as OCTA, PS-OCT, OCE, PhD-OCT, PT-OCT, and PP-OCT, aim to add additional contrast to conventional OCT images. The complementary en face and cross-sectional information from combined SLO and OCT systems has benefited motion-tracking and aiming in clinical ophthalmology, and the addition of AO and fluorescence methods has further improved resolution and imaging specificity. Integration of OCT with surgical microscopy has benefited real-time surgical feedback and surgical decision-making. Finally, multimodal photoacoustic imaging systems enable quantitative imaging of blood perfusion and *in vivo* hemodynamics. Overall, multimodal ophthalmic imaging developments have led to improvements in clinical imaging and novel

basic science research with new possibilities for clinical translation and improvements in disease diagnosis and therapeutic monitoring.

Acknowledgement

Morgan J. Ringel and Eric M. Tang contributed equally.

Conflict of interest statement

The authors declared no potential conflicts of interest with respect to the research, authorship, and/or publication of this article.

Funding

The authors disclosed receipt of the following financial support for the research, authorship, and/or publication of this article: This research was supported by Vanderbilt University, the Vanderbilt Institute for Surgery and Engineering (VISE), and the US National Institutes of Health Grant No. R01-EY030490, R01-EY031769 and T32-EB021937. The content was solely the responsibility of the authors and does not necessarily represent the official views of the National Institutes of Health.

ORCID iD

Yuankai K. Tao https://orcid.org/0000-0002-6135-6241

References

1. Webb RH, Hughes GW and Pomerantzeff O. Flying spot TV ophthalmoscope. *Appl Opt* 1980; 19: 2991–2997.
2. Webb RH and Hughes GW. Scanning laser ophthalmoscope. *IEEE Trans Biomed Eng* 1981; 28: 488–492.
3. Patel SN, Shi A, Wibbelsman TD, *et al.* Ultra-widefield retinal imaging: an update on recent advances. *Ther Adv Ophthalmol* 2020; 12: 1–12.
4. Huang D, Swanson EA, Lin CP, *et al.* Optical coherence tomography. *Science* 1991; 254: 1178–1181.
5. Liang J, Williams DR and Miller DT. Supernormal vision and high-resolution retinal imaging through adaptive optics. *J Opt Soc Am A Opt Image Sci Vis* 1997; 14: 2884–2892.
6. de Carlo TE, Romano A, Waheed NK, *et al.* A review of optical coherence tomography angiography (OCTA). *Int J Retina Vitreous* 2015; 1: 5.
7. Spaide RF, Fujimoto JG, Waheed NK, *et al.* Optical coherence tomography angiography. *Prog Retin Eye Res* 2018; 64: 1–55.
8. Spaide RF, Klancnik JM Jr and Cooney MJ. Retinal vascular layers imaged by fluorescein angiography and optical coherence tomography angiography. *JAMA Ophthalmol* 2015; 133: 45–50.
9. Makita S, Hong Y, Yamanari M, *et al.* Optical coherence angiography. *Opt Express* 2006; 14: 7821–7840.
10. Wang RK, Jacques SL, Ma Z, *et al.* Three dimensional optical angiography. *Opt Express* 2007; 15: 4083–4097.
11. An L and Wang RK. In vivo volumetric imaging of vascular perfusion within human retina and choroids with optical micro-angiography. *Opt Express* 2008; 16: 11438–11452.
12. Fingler J, Zawadzki RJ, Werner JS, *et al.* Volumetric microvascular imaging of human retina using optical coherence tomography with a novel motion contrast technique. *Opt Express* 2009; 17: 22190–22200.
13. Yu L and Chen Z. Doppler variance imaging for three-dimensional retina and choroid angiography. *J Biomed Opt* 2010; 15: 016029.
14. Jia Y, Tan O, Tokayer J, *et al.* Split-spectrum amplitude-decorrelation angiography with optical coherence tomography. *Opt Express* 2012; 20: 4710–4725.
15. Mariampillai A, Standish BA, Moriyama EH, *et al.* Speckle variance detection of microvasculature using swept-source optical coherence tomography. *Opt Lett* 2008; 33: 1530–1532.
16. Jia Y, Morrison JC, Tokayer J, *et al.* Quantitative OCT angiography of optic nerve head blood flow. *Biomed Opt Express* 2012; 3: 3127–3137.
17. Jia Y, Wei E, Wang X, *et al.* Optical coherence tomography angiography of optic disc perfusion in glaucoma. *Ophthalmology* 2014; 121: 1322–1332.
18. Jia Y, Baileya ST, Hwanga TS, *et al.* Quantitative optical coherence tomography angiography of vascular abnormalities in the living human eye. *Proc Natl Acad Sci USA* 2015; 112: E2395–E2402.
19. Liu G, Jia Y, Pechauer AD, *et al.* Split-spectrum phase-gradient optical coherence tomography angiography. *Biomed Opt Express* 2016; 7: 2943–2954.
20. Nam AS, Chico-Calero I and Vakoc BJ. Complex differential variance algorithm for optical coherence tomography angiography. *Biomed Opt Express* 2014; 5: 3822–3832.

21. Braaf B, Donner S, Nam AS, *et al*. Complex differential variance angiography with noise-bias correction for optical coherence tomography of the retina. *Biomed Opt Express* 2018; 9: 486–506.

22. Yousefi S, Zhi Z and Wang RK. Eigendecomposition-based clutter filtering technique for optical microangiography. *IEEE Trans Biomed Eng* 2011; 58: 2316–2323.

23. An L, Shen TT and Wang RK. Using ultrahigh sensitive optical microangiography to achieve comprehensive depth resolved microvasculature mapping for human retina. *J Biomed Opt* 2011; 16: 106013.

24. Chung CS, Nesper PL, Park JJ, *et al*. Comparison of Zeiss cirrus and Optovue RTVue OCT angiography systems: a quantitative and qualitative approach examining the three capillary networks in diabetic retinopathy. *Ophthalmic Surg Lasers Imaging Retin* 2018; 49: E198–E205.

25. Jung W, Kim J, Jeon M, *et al*. Handheld optical coherence tomography scanner for primary care diagnostics. *IEEE Trans Biomed Eng* 2011; 58: 741–744.

26. Lu CD, Kraus MF, Potsaid B, *et al*. Handheld ultrahigh speed swept source optical coherence tomography instrument using a MEMS scanning mirror. *Biomed Opt Express* 2014; 5: 293–311.

27. Larocca F, Nankivil D, Dubose T, *et al*. In vivo cellular-resolution retinal imaging in infants and children using an ultracompact handheld probe. *Nat Photonics* 2016; 10: 580–584.

28. Yang J, Liu L, Campbell JP, *et al*. Handheld optical coherence tomography angiography. *Biomed Opt Express* 2017; 8: 2287–2300.

29. Campbell JP, Nudleman E, Yang J, *et al*. Handheld optical coherence tomography angiography and ultra-wide-field optical coherence tomography in retinopathy of prematurity. *JAMA Ophthalmol* 2017; 135: 977–981.

30. Malone JD, El-Haddad MT, Yerramreddy SS, *et al*. Handheld spectrally encoded coherence tomography and reflectometry for motion-corrected ophthalmic optical coherence tomography and optical coherence tomography angiography. *Neurophotonics* 2019; 6: 041102.

31. Viehland C, Chen X, Tran-Viet D, *et al*. Ergonomic handheld OCT angiography probe optimized for pediatric and supine imaging. *Biomed Opt Express* 2019; 10: 2623–2638.

32. Song S, Zhou K, Xu JJ, *et al*. Development of a clinical prototype of a miniature hand-held optical coherence tomography probe for prematurity and pediatric ophthalmic imaging. *Biomed Opt Express* 2019; 10: 2383–2398.

33. Yi J and Li X. Estimation of oxygen saturation from erythrocytes by high-resolution spectroscopic optical coherence tomography. *Opt Lett* 2010; 35: 2094–2096.

34. Robles FE, Wilson C, Grant G, *et al*. Molecular imaging true-colour spectroscopic optical coherence tomography. *Nat Photonics* 2011; 5: 744–747.

35. Yi J, Wei Q, Liu W, *et al*. Visible-light optical coherence tomography for retinal oximetry. *Opt Lett* 2013; 38: 1796–1798.

36. Yi J, Chen S, Shu X, *et al*. Human retinal imaging using visible-light optical coherence tomography guided by scanning laser ophthalmoscopy. *Biomed Opt Express* 2015; 6: 3701–3713.

37. Chong SP, Merkle CW, Leahy C, *et al*. Quantitative microvascular hemoglobin mapping using visible light spectroscopic optical coherence tomography. *Biomed Opt Express* 2015; 6: 1429–1450.

38. Chong SP, Bernucci M, Radhakrishnan H, *et al*. Structural and functional human retinal imaging with a fiber-based visible light OCT ophthalmoscope. *Biomed Opt Express* 2017; 8: 323–337.

39. Yu DY and Cringle SJ. Retinal degeneration and local oxygen metabolism. *Exp Eye Res* 2005; 80: 745–751.

40. Nesper PL, Soetikno BT, Zhang HF, *et al*. OCT angiography and visible-light OCT in diabetic retinopathy. *Vision Res* 2017; 139: 191–203.

41. Chen S, Yi J and Zhang HF. Measuring oxygen saturation in retinal and choroidal circulations in rats using visible light optical coherence tomography angiography. *Biomed Opt Express* 2015; 6: 2840–2853.

42. Pi S, Camino A, Zhang M, *et al*. Angiographic and structural imaging using high axial resolution fiber-based visible-light OCT. *Biomed Opt Express* 2017; 8: 4595–4608.

43. Pi S, Camino A, Wei X, *et al*. Rodent retinal circulation organization and oxygen metabolism revealed by visible-light optical coherence tomography. *Biomed Opt Express* 2018; 9: 5851–5862.

44. Pi S, Hormel TT, Wei X, *et al*. Retinal capillary oximetry with visible light optical coherence tomography. *Proc Natl Acad Sci USA* 2020; 117: 11658–11666.

45. Chen S, Shu X, Nesper PL, *et al*. Retinal oximetry in humans using visible-light optical coherence tomography [Invited]. *Biomed Opt Express* 2017; 8: 1415–1429.

46. Chong SP, Zhang T, Kho A, *et al*. Ultrahigh resolution retinal imaging by visible light OCT with longitudinal achromatization. *Biomed Opt Express* 2018; 9: 1477–1491.

47. Rubinoff I, Beckmann L, Wang Y, *et al*. Speckle reduction in visible-light optical coherence tomography using scan modulation. *Neurophotonics* 2019; 6: 041107.

48. Shu X, Beckmann L, Wang Y, *et al*. Designing visible-light optical coherence tomography towards clinics. *Quant Imaging Med Surg* 2019; 9: 769–781.

49. Russell JF, Shi Y, Hinkle JW, *et al*. Longitudinal wide-field swept-source OCT angiography of neovascularization in proliferative diabetic retinopathy after panretinal photocoagulation. *Ophthalmol Retina* 2019; 3: 350–361.

50. Chen H, Chi W, Cai X, *et al*. Macular microvasculature features before and after vitrectomy in idiopathic macular epiretinal membrane: an OCT angiography analysis. *Eye* 2019; 33: 619–628.

51. Sacconi R, Tomasso L, Corbelli E, *et al*. Early response to the treatment of choroidal neovascularization complicating central serous chorioretinopathy: a OCT-angiography study. *Eye* 2019; 33: 1809–1817.

52. Vujosevic S, Toma C, Villani E, *et al*. Diabetic macular edema with neuroretinal detachment: OCT and OCT-angiography biomarkers of treatment response to anti-VEGF and steroids. *Acta Diabetol* 2020; 57: 287–296.

53. Zhang Q, Rezaei KA, Saraf SS, *et al*. Ultra-wide optical coherence tomography angiography in diabetic retinopathy. *Quant Imaging Med Surg* 2018; 8: 743–753.

54. Couturier A, Rey PA, Erginay A, *et al*. Widefield OCT-angiography and fluorescein angiography assessments of nonperfusion in diabetic retinopathy and edema treated with anti–vascular endothelial growth factor. *Ophthalmology* 2019; 126: 1685–1694.

55. Hagag AM, Gao SS, Jia Y, *et al*. Optical coherence tomography angiography: technical principles and clinical applications in ophthalmology. *Taiwan J Ophthalmol* 2017; 7: 115–129.

56. Munk MR, Giannakaki-Zimmermann H, Berger L, *et al*. OCT-angiography: a qualitative and quantitative comparison of 4 OCT-A devices. *PLoS ONE* 2017; 12: e0177059.

57. Bernucci MT, Merkle CW and Srinivasan VJ. Investigation of artifacts in retinal and choroidal OCT angiography with a contrast agent. *Biomed Opt Express* 2018; 9: 1020–1040.

58. Camino A, Jia Y, Yu J, *et al*. Automated detection of shadow artifacts in optical coherence tomography angiography. *Biomed Opt Express* 2019; 10: 1514–1531.

59. Choi WJ, Paulson B, Yu S, *et al*. Mean-subtraction method for de-shadowing of tail artifacts in cerebral OCTA images: a proof of concept. *Materials* 2020; 13: 2024.

60. Holmen IC, Konda MS, Pak JW, *et al*. Prevalence and severity of artifacts in optical coherence tomographic angiograms. *JAMA Ophthalmol* 2020; 138: 119–126.

61. Ferguson RD, Hammer DX, Paunescu LA, *et al*. Tracking optical coherence tomography. *Opt Lett* 2004; 29: 2139–2141.

62. Braaf B, Vienola KV, Sheehy CK, *et al*. Real-time eye motion correction in phase-resolved OCT angiography with tracking SLO. *Biomed Opt Express* 2013; 4: 51–65.

63. Chen S, Lou Z, Chen D, *et al*. An artificial flexible visual memory system based on an UV-motivated memristor. *Adv Mater* 2018; 30: 1705400.

64. Wei X, Hormel TT, Guo Y, *et al*. High-resolution wide-field OCT angiography with a self-navigation method to correct microsaccades and blinks. *Biomed Opt Express* 2020; 11: 3234.

65. Fathi A and Naghsh-Nilchi AR. Automatic wavelet-based retinal blood vessels segmentation and vessel diameter estimation. *Biomed Signal Process Control* 2013; 8: 71–80.

66. Eladawi N, Elmogy M, Helmy O, *et al*. Automatic blood vessels segmentation based on different retinal maps from OCTA scans. *Comput Biol Med* 2017; 89: 150–161.

67. Uji A, Balasubramanian S, Lei J, *et al*. Multiple enface image averaging for enhanced optical coherence tomography angiography imaging. *Acta Ophthalmol* 2018; 96: e820–e827.

68. Chu Z, Zhou H, Cheng Y, *et al*. Improving visualization and quantitative assessment of choriocapillaris with swept source OCTA

through registration and averaging applicable to clinical systems. *Sci Rep* 2018; 8: 1–13.

69. ANSI Z136.1-1993. American national standard for the safe use of lasers.

70. Hee MR, Swanson EA, Fujimoto JG, *et al*. Polarization-sensitive low-coherence reflectometer for birefringence characterization and ranging. *J Opt Soc Am B* 1992; 9: 903–908.

71. Götzinger E, Pircher M, Geitzenauer W, *et al*. Retinal pigment epithelium segmentation by polarization sensitive optical coherence tomography. *Opt Express* 2008; 16: 16410–16422.

72. Götzinger E, Pircher M, Baumann B, *et al*. Three-dimensional polarization sensitive OCT imaging and interactive display of the human retina. *Opt Express* 2009; 17: 4151–4165.

73. de Boer JF, Milner TE, van Gemert MJC, *et al*. Two-dimensional birefringence imaging in biological tissue by polarization-sensitive optical coherence tomography. *Opt Lett* 1997; 22: 934–936.

74. de Boer JF, Milner TE and Nelson JS. Determination of the depth-resolved Stokes parameters of light backscattered from turbid media by use of polarization-sensitive optical coherence tomography. *Opt Lett* 1999; 24: 300–302.

75. Saxer CE, de Boer JF, Park BH, *et al*. High-speed fiber–based polarization-sensitive optical coherence tomography of in vivo human skin. *Opt Lett* 2000; 25: 1355–1357.

76. Jiao S, Yao G and Wang LV. Depth-resolved two-dimensional Stokes vectors of backscattered light and Mueller matrices of biological tissue measured with optical coherence tomography. *Appl Opt* 2000; 39: 6318–6324.

77. Jiao S and Wang LV. Two-dimensional depth-resolved Mueller matrix of biological tissue measured with double-beam polarization-sensitive optical coherence tomography. *Opt Lett* 2002; 27: 101–103.

78. de Boer J, Srinivas S, Malekafzali A, *et al*. Imaging thermally damaged tissue by Polarization Sensitive Optical Coherence Tomography. *Opt Express* 1998; 3: 212–218.

79. Schoenenberger K, Colston BW, Maitland DJ, *et al*. Mapping of birefringence and thermal damage in tissue by use of polarization-sensitive optical coherence tomography. *Appl Opt* 1998; 37: 6026–6036.

80. Maurice DM. The structure and transparency of the cornea. *J Physiol* 1957; 136: 263–286.

81. Ducros MG, De Boer JF, Huang HE, *et al*. Polarization sensitive optical coherence tomography of the rabbit eye. *IEEE J Sel Top Quantum Electron* 1999; 5: 1159–1167.

82. Götzinger E, Pircher M, Sticker M, *et al*. Measurement and imaging of birefringent properties of the human cornea with phase-resolved, polarization-sensitive optical coherence tomography. *J Biomed Opt* 2004; 9: 94–102.

83. Götzinger E, Pircher M, Dejaco-Ruhswurm I, *et al*. Imaging of birefringent properties of keratoconus corneas by polarization-sensitive optical coherence tomography. *Invest Ophthalmol Vis Sci* 2007; 48: 3551–3558.

84. Pircher M, Goetzinger E, Leitgeb R, *et al*. Transversal phase resolved polarization sensitive optical coherence tomography. *Phys Med Biol* 2004; 49: 1257–1263.

85. Miyazawa A, Yamanari M, Makita S, *et al*. Tissue discrimination in anterior eye using three optical parameters obtained by polarization sensitive optical coherence tomography. *Opt Express* 2009; 17: 17426–17440.

86. Yasuno Y, Yamanari M, Kawana K, *et al*. Visibility of trabecular meshwork by standard and polarization-sensitive optical coherence tomography. *J Biomed Opt* 2010; 15: 061705.

87. Yasuno Y, Yamanari M, Kawana K, *et al*. Investigation of post-glaucoma-surgery structures by three-dimensional and polarization sensitive anterior eye segment optical coherence tomography. *Opt Express* 2009; 17: 3980–3996.

88. Fukuda S, Beheregaray S, Kasaragod D, *et al*. Noninvasive evaluation of phase retardation in blebs after glaucoma surgery using anterior segment polarization-sensitive optical coherence tomography. *Invest Ophthalmol Vis Sci* 2014; 55: 5200–5206.

89. Beer F, Wartak A, Pircher N, *et al*. Mapping of corneal layer thicknesses with polarization-sensitive optical coherence tomography using a conical scan pattern. *Invest Ophthalmol Vis Sci* 2018; 59: 5579–5588.

90. Beer F, Patil RP, Sinha-Roy A, *et al*. Ultrahigh resolution polarization sensitive optical coherence tomography of the human cornea with conical scanning pattern and variable dispersion compensation. *Appl Sci* 2019; 9: 4245.

91. Wartak A, Schenk MS, Bühler V, *et al*. Micro-optical coherence tomography for high-resolution morphologic imaging of cellular and nerval corneal micro-structures. *Biomed Opt Express* 2020; 11: 5920–5933.

92. Pircher N, Beer F, Holzer S, *et al*. Large field of view corneal epithelium and Bowman's layer thickness maps in keratoconic and healthy eyes. *Am J Ophthalmol* 2020; 209: 168–177.

93. Ducros MG, Marsack JD, Rylander HG 3rd, *et al*. Primate retina imaging with polarization-sensitive optical coherence tomography. *J Opt Soc Am A Opt Image Sci Vis* 2001; 18: 2945–2956.

94. Cense B, Chen TC, Park BH, *et al*. Thickness and birefringence of healthy retinal nerve fiber layer tissue measured with polarization-sensitive optical coherence tomography. *Invest Ophthalmol Vis Sci* 2004; 45: 2606–2612.

95. Cense B, Chen TC, Park BH, *et al*. In vivo birefringence and thickness measurements of the human retinal nerve fiber layer using polarization-sensitive optical coherence tomography. *J Biomed Opt* 2004; 9: 121–125.

96. Zhou Q and Knighton RW. Light scattering and form birefringence of parallel cylindrical arrays that represent cellular organelles of the retinal nerve fiber layer. *Appl Opt* 1997; 36: 2273–2285.

97. Yamanari M, Miura M, Makita S, *et al*. Phase retardation measurement of retinal nerve fiber layer by polarization-sensitive spectral-domain optical coherence tomography and scanning laser polarimetry. *J Biomed Opt* 2008; 13: 014013.

98. Desissaire S, Pollreisz A, Sedova A, *et al*. Analysis of retinal nerve fiber layer birefringence in patients with glaucoma and diabetic retinopathy by polarization sensitive OCT. *Biomed Opt Express* 2020; 11: 5488–5505.

99. Pircher M, Götzinger E, Leitgeb R, *et al*. Imaging of polarization properties of human retina in vivo with phase resolved transversal PS-OCT. *Opt Express* 2004; 12: 5940–5951.

100. Pircher M, Götzinger E, Findl O, *et al*. Human macula investigated in vivo with polarization-sensitive optical coherence tomography. *Invest Ophthalmol Vis Sci* 2006; 47: 5487–5494.

101. Baumann B, Götzinger E, Pircher M, *et al*. Measurements of depolarization distribution in the healthy human macula by polarization sensitive OCT. *J Biophotonics* 2009; 2: 426–434.

102. Baumann B, Gotzinger E, Pircher M, *et al*. Segmentation and quantification of retinal lesions in age-related macular degeneration using polarization-sensitive optical coherence tomography. *J Biomed Opt* 2010; 15: 061704.

103. Cense B, Gao W, Brown JM, *et al*. Retinal imaging with polarization-sensitive optical coherence tomography and adaptive optics. *Opt Express* 2009; 17: 21634–21651.

104. Schlanitz FG, Sacu S, Baumann B, *et al*. Identification of Drusen characteristics in age-related macular degeneration by polarization-sensitive optical coherence tomography. *Am J Ophthalmol* 2015; 160: 335–344.e1.

105. Cense B, Miller DT, King BJ, *et al*. Measuring polarization changes in the human outer retina with polarization-sensitive optical coherence tomography. *J Biophotonics* 2018; 11: e201700134.

106. Roberts P, Sugita M, Deák G, *et al*. Automated identification and quantification of subretinal fibrosis in neovascular age-related macular degeneration using polarization-sensitive OCT. *Invest Ophthalmol Vis Sci* 2016; 57: 1699–1705.

107. Gräfe MGO, van de Kreeke JA, Willemse J, *et al*. Subretinal fibrosis detection using polarization sensitive optical coherence tomography. *Transl Vis Sci Technol* 2020; 9: 13.

108. Gong P, Li Q, Wang Q, *et al*. Jones matrix-based speckle-decorrelation angiography using polarization-sensitive optical coherence tomography. *J Biophotonics* 2020; 13: e202000007.

109. de Boer JF, Hitzenberger CK and Yasuno Y. Polarization sensitive optical coherence tomography—a review [Invited]. *Biomed Opt Express* 2017; 8: 1838–1873.

110. Baumann B. Polarization sensitive optical coherence tomography: a review of technology and applications. *Appl Sci* 2017; 7: 474.

111. Azuma S, Makita S, Miyazawa A, *et al*. Pixel-wise segmentation of severely pathologic retinal pigment epithelium and choroidal stroma using multi-contrast Jones matrix optical coherence tomography. *Biomed Opt Express* 2018; 9: 2955–2973.

112. Miura M, Makita S, Azuma S, *et al*. Evaluation of focal damage in the retinal pigment epithelium layer in serous retinal pigment epithelium detachment. *Sci Rep* 2019; 9: 3278.

113. Lerner RM, Parker KJ, Holen J, *et al*. Sono-elasticity: medical elasticity images derived from ultrasound signals in mechanically vibrated targets. In: Kessler LW (eds) *Acoustical imaging*. Boston, MA: Springer, 1988, pp. 317–327.

114. Kennedy BF, Kennedy KM and Sampson DD. A review of optical coherence elastography: fundamentals, techniques and prospects. *IEEE J Sel Top Quantum Electron* 2014; 20: 272–288.

115. Chhetri RK, Kozek KA, Johnston-Peck AC, *et al*. Imaging three-dimensional rotational diffusion of plasmon resonant gold nanorods using polarization-sensitive optical coherence tomography. *Phys Rev E Stat Nonlin Soft Matter Phys* 2011; 83: 040903.

116. Blackmon RL, Sandhu R, Chapman BS, *et al*. Imaging extracellular matrix remodeling in vitro by diffusion-sensitive optical coherence tomography. *Biophys J* 2016; 110: 1858–1868.

117. Blackburn BJ, Gu S, Ford MR, *et al*. Noninvasive assessment of corneal crosslinking with phase-decorrelation optical coherence tomography. *Invest Ophthalmol Vis Sci* 2019; 60: 41–51.

118. Schmitt JM. OCT elastography: imaging microscopic deformation and strain of tissue. *Opt Express* 1998; 3: 199–211.

119. Chen EJ, Novakofski J, Kenneth Jenkins W, *et al*. Young's modulus measurements of soft tissues with application to elasticity imaging. *IEEE Trans Ultrason Ferroelectr Freq Control* 1996; 43: 191–194.

120. Liang X, Crecea V and Boppart SA. Dynamic optical coherence elastography: a review. *J Innov Opt Health Sci* 2010; 3: 221–233.

121. Ramier A, Eltony AM, Chen YT, *et al*. In vivo measurement of shear modulus of the human cornea using optical coherence elastography. *Sci Rep* 2020; 10: 17366.

122. Sridhar MS. Anatomy of cornea and ocular surface. *Indian J Ophthalmol* 2018; 66: 190–194.

123. Roberts CJ and Dupps WJ Jr. Biomechanics of corneal ectasia and biomechanical treatments. *J Cataract Refract Surg* 2014; 40: 991–998.

124. Hong CW, Sinha-Roy A, Schoenfield L, *et al*. Collagenase-mediated tissue modeling of corneal ectasia and collagen cross-linking treatments. *Invest Ophthalmol Vis Sci* 2012; 53: 2321–2327.

125. Wollensak G, Spoerl E and Seiler T. Riboflavin/ultraviolet-A-induced collagen crosslinking for the treatment of keratoconus. *Am J Ophthalmol* 2003; 135: 620–627.

126. Dascalescu D, Corbu C, Vasile P, *et al*. The importance of assessing corneal biomechanical properties in glaucoma patients care—a review. *Rom J Ophthalmol* 2016; 60: 219–225.

127. Zhou Y, Wang Y, Shen M, *et al*. In vivo evaluation of corneal biomechanical properties by optical coherence elastography at different cross-linking irradiances. *J Biomed Opt* 2019; 24: 105001.

128. Singh M, Li J, Vantipalli S, *et al*. Noncontact elastic wave imaging optical coherence elastography for evaluating changes in corneal elasticity due to crosslinking. *IEEE J Sel Top Quantum Electron* 2016; 22: 6801911.

129. Han Z, Li J, Singh M, *et al*. Analysis of the effect of the fluid-structure interface on elastic wave velocity in cornea-like structures by OCE and FEM. *Laser Phys Lett* 2016; 13: 035602.

130. Ambroziński Ł, Pelivanov I, Song S, *et al*. Air-coupled acoustic radiation force for non-contact generation of broadband mechanical waves in soft media. *Appl Phys Lett* 2016; 109: 043701.

131. Jin ZI, Khazaeinezhad R, Zhu J, *et al*. In-vivo 3D corneal elasticity using air-coupled ultrasound optical coherence elastography. *Biomed Opt Express* 2019; 10: 6272–6285.

132. Ambroziński Ł, Song S, Yoon SJ, *et al*. Acoustic micro-tapping for non-contact 4D imaging of tissue elasticity. *Sci Rep* 2016; 6: 38967.

133. Pitre JJ, Kirby MA, Li DS, *et al*. Nearly-incompressible transverse isotropy (NITI) of cornea elasticity: model and experiments with acoustic micro-tapping OCE. *Sci Rep* 2020; 10: 12983.

134. Qu Y, Ma T, He Y, *et al*. Acoustic radiation force optical coherence elastography of corneal tissue HHS public access. *IEEE J Sel Top Quantum Electron* 2016; 22: 6803507.

135. Nair A, Singh M, Aglyamov SR, *et al*. Heartbeat OCE: corneal biomechanical response to simulated heartbeat pulsation measured by optical coherence elastography. *J Biomed Opt* 2020; 25: 055001.

136. Li C, Guan G, Huang Z, *et al*. Noncontact all-optical measurement of corneal elasticity. *Opt Lett* 2012; 37: 1625–1627.

137. Tabandeh H, Thompson GM, Heyworth P, *et al*. Water content, lens hardness and cataract appearance. *Eye* 1994; 8: 125–129.

138. Li Y, Zhu J, Chen JJ, *et al*. Simultaneously imaging and quantifying in vivo mechanical properties of crystalline lens and cornea using optical coherence elastography with acoustic radiation force excitation. *APL Photonics* 2019; 4: 106104.

139. Ambekar YS, Singh M, Zhang J, *et al*. Multimodal quantitative optical elastography of the crystalline lens with optical coherence elastography and Brillouin microscopy. *Biomed Opt Express* 2020; 11: 2041–2051.

140. Zhang H, Larin KV, Aglyamov SR, *et al*. Quantifying lens elastic properties with

optical coherence elastography as a function of intraocular pressure. In: Larin KV and Scarcelli G (eds) *Optical elastography and tissue biomechanics VI*. Bellingham, WA: SPIE, 2019, p. 60.

141. Krishnan L, Hoying JB, Nguyen H, *et al*. Interaction of angiogenic microvessels with the extracellular matrix. *Am J Physiol Circ Physiol* 2007; 293: H3650–H3658.

142. Qu Y, He Y, Zhang Y, *et al*. Quantified elasticity mapping of retinal layers using synchronized acoustic radiation force optical coherence elastography. *Biomed Opt Express* 2018; 9: 4054–4063.

143. Qu Y, He Y, Saidi A, *et al*. In vivo elasticity mapping of posterior ocular layers using acoustic radiation force optical coherence elastography. *Invest Ophthalmol Vis Sci* 2018; 59: 455–461.

144. Du Z, Li R, Qian X, *et al*. Quantitative confocal optical coherence elastography for evaluating biomechanics of optic nerve head using Lamb wave model. *Neurophotonics* 2019; 6: 041112.

145. Singh M, Nair A, Aglyamov SR, *et al*. Noncontact optical coherence elastography of the posterior porcine sclera in situ as a function of IOP. In: Manns F, Söderberg PG and Ho A (eds) *Ophthalmic technologies XXVII*. Bellingham, WA: SPIE, 2017, p. 1004524.

146. Kirby MA, Pelivanov I, Song S, *et al*. Optical coherence elastography in ophthalmology. *J Biomed Opt* 2017; 22: 1–28.

147. Singh M, Wu C, Liu C-H, *et al*. Phase-sensitive optical coherence elastography at 15 million A-Lines per second. *Opt Lett* 2015; 40: 2588–2591.

148. Gordon AY, Lapierre-Landry M, Skala MC, *et al*. Photothermal optical coherence tomography of anti-angiogenic treatment in the mouse retina using gold nanorods as contrast agents. *Transl Vis Sci Technol* 2019; 8: 18.

149. Adler DC, Huang S-W, Huber R, *et al*. Photothermal detection of gold nanoparticles using phase-sensitive optical coherence tomography. *Opt Express* 2008; 16: 4376–4393.

150. Lapierre-Landry M, Gordon AY, Penn JS, *et al*. In vivo photothermal optical coherence tomography of endogenous and exogenous contrast agents in the eye. *Sci Rep* 2017; 7: 9228.

151. Lapierre-Landry M, Huckenpahler AL, Link BA, *et al*. Imaging melanin distribution in the zebrafish retina using photothermal optical coherence tomography. *Transl Vis Sci Technol* 2018; 7: 4.

152. Lapierre-Landry M, Connor TB, Carroll J, *et al*. Photothermal optical coherence tomography of indocyanine green in ex vivo eyes. *Opt Lett* 2018; 43: 2470–2473.

153. Rao KD, Choma MA, Yazdanfar S, *et al*. Molecular contrast in optical coherence tomography by use of a pump-probe technique. *Opt Lett* 2003; 28: 340–342.

154. Carrasco-Zevallos O, Shelton RL, Kim W, *et al*. In vivo pump-probe optical coherence tomography imaging in *Xenopus laevis*. *J Biophotonics* 2015; 8: 25–35.

155. Jacob D, Shelton RL and Applegate BE. Fourier domain pump-probe optical coherence tomography imaging of melanin. In: *2009 conference on lasers and electro-optics and 2009 conference on quantum electronics and laser science conference (CLEO/QELS 2009)*, Baltimore, MD, 2–4 June 2009, p. 12399. Washington, DC: Optical Society of America.

156. Pircher M, Baumann B, Götzinger E, *et al*. Simultaneous SLO/OCT imaging of the human retina with axial eye motion correction. *Opt Express* 2007; 15: 16922–16932.

157. Pircher M, Götzinger E, Sattmann H, *et al*. In vivo investigation of human cone photoreceptors with SLO/OCT in combination with 3D motion correction on a cellular level. *Opt Express* 2010; 18: 13935–13944.

158. Vienola KV, Braaf B, Sheehy CK, *et al*. Real-time eye motion compensation for OCT imaging with tracking SLO. *Biomed Opt Express* 2012; 3: 2950–2963.

159. Schwarzhans F, Desissaire S, Steiner S, *et al*. Generating large field of view en-face projection images from intra-acquisition motion compensated volumetric optical coherence tomography data. *Biomed Opt Express* 2020; 11: 6881–6904.

160. Podoleanu AG and Jackson DA. Combined optical coherence tomograph and scanning laser ophthalmoscope. *Electron Lett* 1998; 34: 1088–1090.

161. Podoleanu AG, Dobre GM, Cucu RG, *et al*. Sequential optical coherence tomography and confocal imaging. *Opt Lett* 2004; 29: 364–366.

162. Hammer DX, Iftimia NV, Ustun TE, *et al*. Dual OCT/SLO imager with three-dimensional tracker. In: Manns F, Soederberg PG and Ho A (eds) *Ophthalmic technologies XV*. Bellingham, WA: SPIE, 2005, p. 33.

163. Iftimia NV, Hammer DX, Bigelow CE, *et al*. Hybrid retinal imager using line-scanning laser ophthalmoscopy and spectral domain optical coherence tomography. *Opt Express* 2006; 14: 12909–12914.

164. Hammer DX, Ferguson RD, Ustun TE, *et al*. Line-scanning laser ophthalmoscope. *J Biomed Opt* 2006; 11: 041126.

165. Malone JD, El-Haddad MT, Bozic I, *et al*. Simultaneous multimodal ophthalmic imaging using swept-source spectrally encoded scanning laser ophthalmoscopy and optical coherence tomography. *Biomed Opt Express* 2017; 8: 193–206.

166. El-Haddad MT, Bozic I and Tao YK. Spectrally encoded coherence tomography and reflectometry: simultaneous en face and cross-sectional imaging at 2 gigapixels per second. *J Biophotonics* 2018; 11: e201700268.

167. Larocca F, Nankivil D, Farsiu S, *et al*. Handheld simultaneous scanning laser ophthalmoscopy and optical coherence tomography system. *Biomed Opt Express* 2013; 4: 2307–2321.

168. LaRocca F, Nankivil D, Farsiu S, *et al*. True color scanning laser ophthalmoscopy and optical coherence tomography handheld probe. *Biomed Opt Express* 2014; 5: 3204–3216.

169. Tao YK and Izatt JA. Spectrally encoded confocal scanning laser ophthalmoscopy. *Opt Lett* 2010; 35: 574–576.

170. Tao YK, Farsiu S and Izatt JA. Interlaced spectrally encoded confocal scanning laser ophthalmoscopy and spectral domain optical coherence tomography. *Biomed Opt Express* 2010; 1: 431–400.

171. Pircher M and Zawadzki RJ. Review of adaptive optics OCT (AO-OCT): principles and applications for retinal imaging [Invited]. *Biomed Opt Express* 2017; 8: 2536–2562.

172. Roorda A, Romero-Borja F, Donnelly III WJ, *et al*. Adaptive optics scanning laser ophthalmoscopy. *Opt Express* 2002; 10: 405–412.

173. Miller DT, Qu J, Jonnal RS, *et al*. Coherence gating and adaptive optics in the eye. In: Tuchin VV, Izatt JA and Fujimoto JG (eds) *Coherence domain optical methods and optical coherence tomography in biomedicine VII*. Bellingham, WA: SPIE, 2003, p. 65.

174. Hermann B, Fernández EJ, Unterhuber A, *et al*. Adaptive-optics ultrahigh-resolution optical coherence tomography. *Opt Lett* 2004; 29: 2142–2144.

175. Dubra A and Sulai Y. Reflective afocal broadband adaptive optics scanning ophthalmoscope. *Biomed Opt Express* 2011; 2: 1757–1768.

176. Mujat M, Ferguson RD, Patel AH, *et al*. High resolution multimodal clinical ophthalmic imaging system. *Opt Express* 2010; 18: 11607–11621.

177. Stevenson SB and Roorda A. Correcting for miniature eye movements in high-resolution scanning laser ophthalmoscopy. In: Manns F, Soederberg PG and Ho A (eds) *Ophthalmic technologies XV*. Bellingham, WA: SPIE, 2005, p. 12.

178. Vogel CR, Arathorn DW, Roorda A, *et al*. Retinal motion estimation in adaptive optics scanning laser ophthalmoscopy. *Opt Express* 2006; 14: 487–497.

179. Cunefare D, Huckenpahler AL, Patterson EJ, *et al*. RAC-CNN: multimodal deep learning based automatic detection and classification of rod and cone photoreceptors in adaptive optics scanning light ophthalmoscope images. *Biomed Opt Express* 2019; 10: 3815–3832.

180. Wang Y, Bensaid N, Tiruveedhula P, *et al*. Human foveal cone photoreceptor topography and its dependence on eye length. *Elife* 2019; 8: e47148.

181. Duncan JL, Zhang Y, Gandhi J, *et al*. High-resolution imaging with adaptive optics in patients with inherited retinal degeneration. *Invest Ophthalmol Vis Sci* 2007; 48: 3283–3291.

182. Genead MA, Fishman GA, Rha J, *et al*. Photoreceptor structure and function in patients with congenital achromatopsia. *Invest Ophthalmol Vis Sci* 2011; 52: 7298–7308.

183. Song H, Rossi EA, Latchney L, *et al*. Cone and rod loss in Stargardt disease revealed by adaptive optics scanning light ophthalmoscopy. *JAMA Ophthalmol* 2015; 133: 1198–1203.

184. Sun LW, Johnson RD, Langlo CS, *et al*. Assessing photoreceptor structure in retinitis pigmentosa and usher syndrome. *Invest Ophthalmol Vis Sci* 2016; 57: 2428–2442.

185. Bennett J, Wellman J, Marshall KA, *et al*. Safety and durability of effect of contralateral-eye administration of AAV2 gene therapy in patients with childhood-onset blindness caused by RPE65 mutations: a follow-on phase 1 trial. *Lancet* 2016; 388: 661–672.

186. Zhang Y, Rha J, Jonnal RS, *et al*. Adaptive optics parallel spectral domain optical coherence tomography for imaging the living retina. *Opt Express* 2005; 13: 4792–4811.

187. Zawadzki RJ, Jones SM, Olivier SS, *et al*. Adaptive-optics optical coherence tomography for high-resolution and high-speed 3D retinal in vivo imaging. *Opt Express* 2005; 13: 8532–8546.

188. Zhang Y, Cense B, Rha J, *et al*. High-speed volumetric imaging of cone photoreceptors with adaptive optics spectral-domain optical coherence tomography. *Opt Express* 2006; 14: 4380–4394.

189. Hammer DX, Ferguson RD, Bigelow CE, *et al*. Adaptive optics scanning laser ophthalmoscope for stabilized retinal imaging. *Opt Express* 2006; 14: 3354–3367.

190. Fernández EJ, Hermann B, Považay B, *et al*. Ultrahigh resolution optical coherence tomography and pancorrection for cellular imaging of the living human retina. *Opt Express* 2008; 16: 11083–11094.

191. Torti C, Považay B, Hofer B, *et al*. Adaptive optics optical coherence tomography at 120,000 depth scans/s for non-invasive cellular phenotyping of the living human retina. *Opt Express* 2009; 17: 19382–19400.

192. Kocaoglu OP, Lee S, Jonnal RS, *et al*. Imaging cone photoreceptors in three dimensions and in time using ultrahigh resolution optical coherence tomography with adaptive optics. *Biomed Opt Express* 2011; 2: 748–763.

193. Kocaoglu OP, Cense B, Jonnal RS, *et al*. Imaging retinal nerve fiber bundles using optical coherence tomography with adaptive optics. *Vision Res* 2011; 51: 1835–1844.

194. Hammer DX, Iftimia NV, Ferguson RD, *et al*. Foveal fine structure in retinopathy of prematurity: an adaptive optics Fourier domain optical coherence tomography study. *Invest Ophthalmol Vis Sci* 2008; 49: 2061–2070.

195. Choi SS, Zawadzki RJ, Lim MC, *et al*. Evidence of outer retinal changes in glaucoma patients as revealed by ultrahigh-resolution in vivo retinal imaging. *Br J Ophthalmol* 2011; 95: 131–141.

196. Panorgias A, Zawadzki RJ, Capps AG, *et al*. Multimodal assessment of microscopic morphology and retinal function in patients with geographic atrophy. *Invest Ophthalmol Vis Sci* 2013; 54: 4372–4384.

197. Nadler Z, Wang B, Schuman JS, *et al*. In vivo three-dimensional characterization of the healthy human lamina cribrosa with adaptive optics spectral-domain optical coherence tomography. *Invest Ophthalmol Vis Sci* 2014; 55: 6459–6466.

198. Dong ZM, Wollstein G, Wang B, *et al*. Adaptive optics optical coherence tomography in glaucoma. *Prog Retin Eye Res* 2017; 57: 76–88.

199. Ferguson RD, Zhong Z, Hammer DX, *et al*. Adaptive optics scanning laser ophthalmoscope with integrated wide-field retinal imaging and tracking. *J Opt Soc Am A Opt Image Sci Vis* 2010; 27: A265–A277.

200. Felberer F, Kroisamer J-S, Baumann B, *et al*. Adaptive optics SLO/OCT for 3D imaging of human photoreceptors in vivo. *Biomed Opt Express* 2014; 5: 439–456.

201. Wells-Gray EM, Choi SS, Zawadzki RJ, *et al*. Volumetric imaging of rod and cone photoreceptor structure with a combined adaptive optics-optical coherence tomography-scanning laser ophthalmoscope. *J Biomed Opt* 2018; 23: 1–15.

202. Stevenson SB, Roorda A and Kumar G. Eye tracking with the adaptive optics scanning laser ophthalmoscope. In: *Eye tracking research and applications symposium (ETRA)*. New York: *ACM Press*, 2010, pp. 195–198.

203. Sheehy CK, Tiruveedhula P, Sabesan R, *et al*. Active eye-tracking for an adaptive optics scanning laser ophthalmoscope. *Biomed Opt Express* 2015; 6: 2412–2423.

204. Chui TY, Song H and Burns SA. Adaptive-optics imaging of human cone photoreceptor distribution. *J Opt Soc Am A Opt Image Sci Vis* 2008; 25: 3021–3029.

205. Dubra A, Sulai Y, Norris JL, *et al*. Noninvasive imaging of the human rod photoreceptor mosaic using a confocal adaptive optics scanning ophthalmoscope. *Biomed Opt Express* 2011; 2: 1864–1876.

206. Doble N, Choi SS, Codona JL, *et al*. In vivo imaging of the human rod photoreceptor mosaic. *Opt Lett* 2011; 36: 31–33.

207. Cunefare D, Langlo CS, Patterson EJ, *et al*. Deep learning based detection of cone photoreceptors with multimodal adaptive optics scanning light ophthalmoscope images of achromatopsia. *Biomed Opt Express* 2018; 9: 3740–3756.

208. Felberer F, Rechenmacher M, Haindl R, *et al*. Imaging of retinal vasculature using adaptive optics SLO/OCT. *Biomed Opt Express* 2015; 6: 1407–1418.

209. Liu Z, Tam J, Saeedi O, *et al*. Trans-retinal cellular imaging with multimodal adaptive optics. *Biomed Opt Express* 2018; 9: 4246–4262.

210. Zhang F, Kurokawa K, Lassoued A, *et al*. Cone photoreceptor classification in the living human eye from photostimulation-induced phase dynamics. *Proc Natl Acad Sci USA* 2019; 116: 7951–7956.

211. Seeliger MW, Beck SC, Pereyra-Muñoz N, *et al*. In vivo confocal imaging of the retina in animal models using scanning laser ophthalmoscopy. *Vision Res* 2005; 45: 3512–3519.

212. Zawadzki RJ, Zhang P, Zam A, *et al*. Adaptive-optics SLO imaging combined with widefield OCT and SLO enables precise 3D localization of fluorescent cells in the mouse retina. *Biomed Opt Express* 2015; 6: 2191–2210.

213. Zhang P, Zam A, Jian Y, *et al*. In vivo wide-field multispectral scanning laser ophthalmoscopy–optical coherence tomography mouse retinal imager: longitudinal imaging of ganglion cells, microglia, and Müller glia, and mapping of the mouse retinal and choroidal vasculature. *J Biomed Opt* 2015; 20: 126005.

214. Gong Y, Li J, Sun Y, *et al*. Optimization of an image-guided laser-induced choroidal neovascularization model in mice. *PLoS ONE* 2015; 10: e0132643.

215. Soetikno BT, Shu X, Liu Q, *et al*. Optical coherence tomography angiography of retinal vascular occlusions produced by imaging-guided laser photocoagulation. *Biomed Opt Express* 2017; 8: 3571–3582.

216. Tao YK, Benavides OR, Terrones BD, *et al*. Multimodality optical coherence tomography and fluorescence confocal scanning laser ophthalmoscopy for image-guided feedback of intraocular injections in mouse models In: Manns F, Söderberg PG and Ho A (eds) *Ophthalmic technologies XXVIII*. Bellingham, WA: SPIE, 2018, p. 51.

217. Malone JD, Levine EM and Tao YK. OCT and fluorescence SLO for guided laser delivery and longitudinal imaging in a murine model of targeted retinal laser injury. In: Manns F, Söderberg PG and Ho A (eds) Ophthalmic *technologies* XXX. Bellingham, WA: SPIE, 2020, p. 49.

218. Zhang L, Song W, Shao D, *et al*. Volumetric fluorescence retinal imaging in vivo over a 30-degree field of view by oblique scanning laser ophthalmoscopy (oSLO). *Biomed Opt Express* 2018; 9: 25–40.

219. Gray DC, Merigan W, Wolfing JI, *et al*. In vivo fluorescence imaging of primate retinal ganglion cells and retinal pigment epithelial cells. *Opt Express* 2006; 14: 7144–7158.

220. Biss DP, Sumorok D, Burns SA, *et al*. In vivo fluorescent imaging of the mouse retina using adaptive optics. *Opt Lett* 2007; 32: 659–661.

221. Hunter JJ, Masella B, Dubra A, *et al*. Images of photoreceptors in living primate eyes using adaptive optics two-photon ophthalmoscopy. *Biomed Opt Express* 2011; 2: 139–148.

222. Sharma R, Yin L, Geng Y, *et al*. In vivo two-photon imaging of the mouse retina. *Biomed Opt Express* 2013; 4: 1285–1293.

223. Palczewska G, Dong Z, Golczak M, *et al*. Noninvasive two-photon microscopy imaging of mouse retina and retinal pigment epithelium through the pupil of the eye. *Nat Med* 2014; 20: 785–789.

224. Qin Z, He S, Yang C, *et al*. Adaptive optics two-photon microscopy enables near-diffraction-limited and functional retinal imaging in vivo. *Light Sci Appl* 2020; 9: 79.

225. Wynne N, Carroll J and Duncan JL. Promises and pitfalls of evaluating retinal diseases with adaptive optics scanning light ophthalmoscopy (AOSLO). *Prog Retin Eye Res* 2020; 2020: 100920.

226. Hofer H, Sredar N, Queener H, *et al*. Wavefront sensorless adaptive optics ophthalmoscopy in the human eye. *Opt Express* 2011; 19: 14160–14171.

227. Jian Y, Xu J, Gradowski MA, *et al*. Wavefront sensorless adaptive optics optical coherence tomography for in vivo retinal imaging in mice. *Biomed Opt Express* 2014; 5: 547–559.

228. Polans J, Keller B, Carrasco-Zevallos OM, *et al*. Wide-field retinal optical coherence tomography with wavefront sensorless adaptive optics for enhanced imaging of targeted regions. *Biomed Opt Express* 2017; 8: 16–37.

229. Wahl DJ, Ng R, Ju MJ, *et al*. Sensorless adaptive optics multimodal en-face small animal retinal imaging. *Biomed Opt Express* 2019; 10: 252–267.

230. Camino A, Zang P, Athwal A, *et al*. Sensorless adaptive-optics optical coherence tomographic angiography. *Biomed Opt Express* 2020; 11: 3952–3967.

231. DuBose T, Nankivil D, LaRocca F, *et al*. Handheld adaptive optics scanning laser ophthalmoscope. *Optica* 2018; 5: 1027–1036.

232. Hagan K, DuBose T, Cunefare D, *et al*. Multimodal handheld adaptive optics scanning laser ophthalmoscope. *Opt Lett* 2020; 45: 4940–4943.

233. Schweitzer D, Hammer M, Schweitzer F, *et al*. In vivo measurement of time-resolved autofluorescence at the human fundus. *J Biomed Opt* 2004; 9: 1214–1222.

234. Dysli C, Wolf S, Berezin MY, *et al*. Fluorescence lifetime imaging ophthalmoscopy. *Prog Retin Eye Res* 2017; 60: 120–143.

235. Feeks JA and Hunter JJ. Adaptive optics two-photon excited fluorescence lifetime imaging ophthalmoscopy of exogenous fluorophores in mice. *Biomed Opt Express* 2017; 8: 2483–2495.

236. Carrasco-Zevallos OM, Viehland C, Keller B, *et al.* Review of intraoperative optical coherence tomography: technology and applications [Invited]. *Biomed Opt Express* 2017; 8: 1607–1637.

237. Boppart SA, Bouma BE, Pitris C, *et al.* Forward-imaging instruments for optical coherence tomography. *Opt Lett* 1997; 22: 1618–1620.

238. Radhakrishnan S, Rollins AM, Roth JE, *et al.* Real-time optical coherence tomography of the anterior segment at 1310 nm. *Arch Ophthalmol* 2001; 119: 1179–1185.

239. Dayani PN, Maldonado R, Farsiu S, *et al.* Intraoperative use of handheld spectral domain optical coherence tomography imaging in macular surgery. *Retina* 2009; 29: 1457–1468.

240. Tao YK, Ehlers JP, Toth CA, *et al.* Intraoperative spectral domain optical coherence tomography for vitreoretinal surgery. *Opt Lett* 2010; 35: 3315–3317.

241. El-Haddad MT and Tao YK. Advances in intraoperative optical coherence tomography for surgical guidance. *Curr Opin Biomed Eng* 2017; 3: 37–48.

242. Carrasco-Zevallos OM, Viehland C, Keller B, *et al.* Constant linear velocity spiral scanning for near video rate 4D OCT ophthalmic and surgical imaging with isotropic transverse sampling. *Biomed Opt Express* 2018; 9: 5052–5070.

243. Carrasco-Zevallos OM, Keller B, Viehland C, *et al.* Live volumetric (4D) visualization and guidance of in vivo human ophthalmic surgery with intraoperative optical coherence tomography. *Sci Rep* 2016; 6: 31689.

244. El-Haddad MT and Tao YK. Automated stereo vision instrument tracking for intraoperative OCT guided anterior segment ophthalmic surgical maneuvers. *Biomed Opt Express* 2015; 6: 3014–3031.

245. Lu CD, Witkin AJ, Waheed NK, *et al.* Ultrahigh speed ophthalmic surgical OCT for intraoperative OCT angiography and widefield imaging. *Invest Ophthalmol Vis Sci* 2016; 57: 466.

246. Viehland C, Vajzovic L, Chen X, *et al.* Intraoperative microscope integrated optical coherence tomography angiography. *Invest Ophthalmol Vis Sci* 2017; 58: 3123.

247. Posarelli C, Sartini F, Casini G, *et al.* What is the impact of intraoperative microscope-integrated OCT in ophthalmic surgery? Relevant applications and outcomes a systematic review. *J Clin Med* 2020; 9: 1682.

248. Ehlers JP, Dupps WJ, Kaiser PK, *et al.* The prospective intraoperative and perioperative ophthalmic imaging with optical CoherEncE TomogRaphy (PIONEER) study: 2-year results. *Am J Ophthalmol* 2014; 158: 999–1007.

249. Ehlers JP, Modi YS, Pecen PE, *et al.* The DISCOVER study 3-year results: feasibility and usefulness of microscope-integrated intraoperative OCT during ophthalmic surgery. *Ophthalmology* 2018; 125: 1014–1027.

250. Ehlers JP, Srivastava SK, Feiler D, *et al.* Integrative advances for OCT-guided ophthalmic surgery and intraoperative OCT: microscope integration, surgical instrumentation, and heads-up display surgeon feedback. *PLoS ONE* 2014; 9: e105224.

251. Rosencwaig A and Gersho A. Theory of the photoacoustic effect with solids. *J Appl Phys* 1976; 47: 64–69.

252. Billeh YN, Liu M and Buma T. Spectroscopic photoacoustic microscopy using a photonic crystal fiber supercontinuum source. *Opt Express* 2010; 18: 18519–18524.

253. Drexler W, Liu M, Kumar A, *et al.* Optical coherence tomography today: speed, contrast, and multimodality. *J Biomed Opt* 2014; 19: 071412.

254. Hu Z, Wang X, Liu Q, *et al.* Photoacoustic imaging in ophthalmology. *Int J Ophthalmol Eye Res* 2015; 3: 126–132.

255. Jiao S, Jiang M, Hu J, *et al.* Photoacoustic ophthalmoscopy for in vivo retinal imaging. *Opt Express* 2010; 18: 3967–3972.

256. Penn JS, Madan A, Caldwell RB, *et al.* Vascular endothelial growth factor in eye disease. *Prog Retin Eye Res* 2008; 27: 331–371.

257. Zhang W, Li Y, Nguyen VP, *et al.* High-resolution, in vivo multimodal photoacoustic microscopy, optical coherence tomography, and fluorescence microscopy imaging of rabbit retinal neovascularization. *Light Sci Appl* 2018; 7: 103.

258. Nguyen VP, Li Y, Aaberg M, *et al.* In vivo 3D imaging of retinal neovascularization using multimodal photoacoustic microscopy and optical coherence tomography imaging. *J Imaging* 2018; 4: 150.

259. Li Y, Zhang W, Nguyen VP, *et al.* Real-time OCT guidance and multimodal imaging monitoring of subretinal injection induced

choroidal neovascularization in rabbit eyes. *Exp Eye Res* 2019; 186: 107714.

260. Nguyen VP, Li Y, Zhang W, *et al*. High-resolution multimodal photoacoustic microscopy and optical coherence tomography image-guided laser induced branch retinal vein occlusion in living rabbits. *Sci Rep* 2019; 9: 10560.

261. Nguyen VP, Li Y, Henry J, *et al*. High resolution multimodal photoacoustic microscopy and optical coherence tomography visualization of choroidal vascular occlusion. *Int J Mol Sci* 2020; 21: 6508.

262. Song W, Wei Q, Liu W, *et al*. A combined method to quantify the retinal metabolic rate of oxygen using photoacoustic ophthalmoscopy and optical coherence tomography. *Sci Rep* 2014; 4: 6525.

263. Fatima A, Kratkiewicz K, Manwar R, *et al*. Review of cost reduction methods in photoacoustic computed tomography. *Photoacoustics* 2019; 15: 100137.

264. Liu X, Liu T, Wen R, *et al*. Optical coherence photoacoustic microscopy for in vivo multimodal retinal imaging. *Opt Lett* 2015; 40: 1370–1373.